EFFECT OF GRAVITY ON SUB-KOLMOGOROV INERTIAL PARTICLES IN A TURBULENT-NON TURBULENT INTERFACE

Julian Reis
Department of Mechanical Engineering
University of Washington
3900 E Stevens Way NE
Seattle, Washington 98195, USA
jreis25@uw.edu

Amélie Ferran
Department of Energy and Process Engineering
NTNU, Trondheim
Strømningsteknisk, 229, Kolbjørn Hejes vei 2
Gløshaugen, Trondheim, Norway
amelie.ferran@ntnu.no

Martin Obligado
Univ. Lille, CNRS, ONERA, Arts et Metiers Institute of Technology
LMFL-Laboratoire de Mécanique des Fluides de Lille
Kampé de Fériet, Centrale Lille, UMR 9014
Lille, F-59000, France
martin.obligado@centralelille.fr

Alberto Aliseda
Department of Mechanical Engineering
University of Washington
3900 E Stevens Way NE
Seattle, Washington 98195, USA
aaliseda@uw.edu

ABSTRACT

Droplet-laden turbulent flows have been studied widely, particularly under homogeneous turbulence, providing a framework to understand particle dynamics in turbulence. Sharp interfaces with different turbulent intensities are found in many particle-laden flows relevant to environmental and industrial applications. For example, Cumulonimbus clouds have sharp interfaces that separate the hot, humid air inside the cloud and the cold, dry ambient air. These interfaces exist both parallel (along the cloud lateral edge) and perpendicular (along the cloud top) to gravity. A better understanding of the behavior of inertial particles immersed in turbulent-non turbulent interfaces would support better understanding and modeling of the complex physical processes involving droplets in warm-rain formation, such as condensation rates in highly inhomogeneous supersaturation fields and collision-coalescence of those inertial condensates. In this experimental study, we investigate the effect of the orientation of the turbulent-non turbulent interface with respect to gravity on the dynamics of inertial particles. We show that gravitational acceleration can enhance particle transport across the turbulent interface, which is dominated by high turbulence entrainment events. Additionally, we show the impact of gravitational acceleration on the statistical moments of particle velocities and accelerations, providing insights into the balance between drag forces and gravity forces across the different cases. Additionally, the analysis of closing velocities between particles also hints at the dynamics of the clustering process.

BACKGROUND

The dynamics of droplet-laden turbulent flows have been studied predominantly in homogeneous isotropic turbulence. Under that condition, studies have found that the settling velocity of inertial particles is enhanced, with the modification increasing with Stokes number (up to peak enhancement at $St = 1$), and with particle loading (Aliseda *et al.* (2002)). Particles interacting with small turbulent scales (Kolmogorov, Taylor) form clusters, and those clusters contribute significantly to the particle dynamics through near-field aerodynamic interactions between particles (Huck *et al.* (2018)). Recent studies have shown that, depending on the Rouse number and the integral length scale, the settling velocity can be either enhanced or hindered by the interaction with the background turbulence (Ferran *et al.* (2023)). Recently, there has been a new focus on the effect of a turbulent-non turbulent interface. In a sheared interface perpendicular to gravity, and therefore not influenced by gravitational acceleration, preferential concentration and settling velocity are enhanced by the turbulent-non turbulent interface (Ferran *et al.* (2024)). In the present study, we focus on the effect of the direction of gravitational acceleration on particles in sheared interfaces. The effect of gravitational acceleration of inertial particles in a turbulent-non-turbulent interface has been looked at in a preliminary study by (Good *et al.* (2012)), in which they reported that intermittent events dominate the transport of particles and generally found inconclusive results on the effect of gravitational acceleration. With new developments in measurement techniques, especially improving the accuracy, length ,and acquisition speed in 3D particle tracking, we build upon previous studies to provide a comprehensive view on the effect of turbulent-non turbulent interfaces and gravity on inertial particle dynamics.

METHODS

Experiments were conducted in a well-characterized low-speed wind tunnel (1 m x 1 m cross-section) at the University of Washington (Seattle, USA). The wind tunnel features an active grid ($M = 0.101$m) with an array of embedded high-speed gas-liquid atomizers. The atomizers produce a droplet size distribution adequate to study cloud droplets formed by condensational growth, with a peak probability around 20µm (Bateson & Aliseda (2012)). The atomizers significantly contribute to the turbulent intensity in the wind tunnel, and therefore, turn-

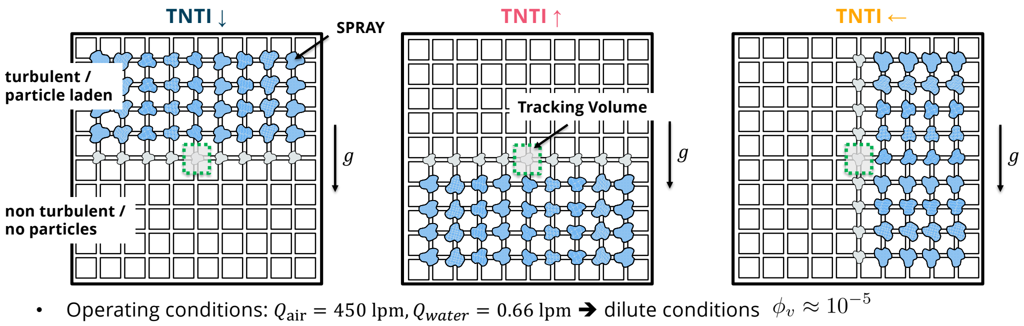

Figure 1. Cross sectional view of the wind tunnel that reveals the atomizer configurations used to create the different turbulent interfaces used for this study. The injectors produce a non-uniform droplet-size distribution and significantly contribute to the turbulent intensity in the wind tunnel. The three cases are: TNTI↓ (top half of injectors turned on - bottom side off), TNTI↑ (bottom half on - top half off), and TNTI← (righ half on - left half off).

ing them off at certain locations generates distinct regions of different turbulent intensity. While keeping the operating conditions constant, we vary the orientation of the turbulent interface by turning off the atomizers on the top or bottom halves of the wind tunnel, or the side of the wind tunnel to create a vertical interface. Fig. 1 shows an overview of the different grid configurations used for these experiments. The different cases are denoted as turbulent/non-turbulent interfaces (TNTI), and the arrow indicates the direction from the turbulent to the non-turbulent stream. This notation is used to reference the cases throughout this paper.

We measure particle dynamics at the theoretical interface location by placing our particle-tracking volume at the center of the wind-tunnel cross section. By combining the beams of two pulsed lasers into a single interrogation volume, we can illuminate a larger volume (110 mm x 70 mm x 40 mm). We can use both pulses to illuminate the particles in 4 consecutive camera frames with $\Delta t = 1$ms, allowing us to measure particle velocities and accelerations in independent snapshots of the flow. The rate of snapshot collection is limited by the laser heads' repetition rate, which in our setup is 10 Hz. The processing steps for the raw camera images include stereo matching and particle tracking (Fig. 2). Using four high-speed cameras provides reliable stereo matching within the 3D volume. For particle tracking, we use the 4BE-ETI particle-tracking algorithm (Clark *et al.* (2019)); its benefit is the enhanced track initialization step, which is essential for our four-frame tracking setup. The algorithm tries to match a particle from the first frame to different particles within an initial search window, whose size can be estimated from the mean flow properties. From the possible matches, the algorithm picks the track that minimizes the particle's overall acceleration, corresponding to the most likely track. An example of a field of particle tracks from a single snapshot is shown in Fig. 2. To better capture the particle's physical trajectory and account for small uncertainties in stereomatching, we fit B-splines to the particle positions. B-splines are smooth up to the second derivative, allowing us to directly evaluate velocities and accelerations from the fitted polynomial. In the statistical analysis of the data, we look at the mean values for each track, e.g., averaging the settling velocity across all 4 positions. With on average $O(10^3)$ tracks per snapshot (TNTI↑: 4150, TNTI↓: 2920, TNTI←: 3410 particles/snapshot), we can sample $O(10^6)$ particle tracks for each case by performing multiple runs, yielding significant statistical datasets.

To correlate carrier flow turbulence statistics with particle dynamics, we need to measure the turbulent flow properties.

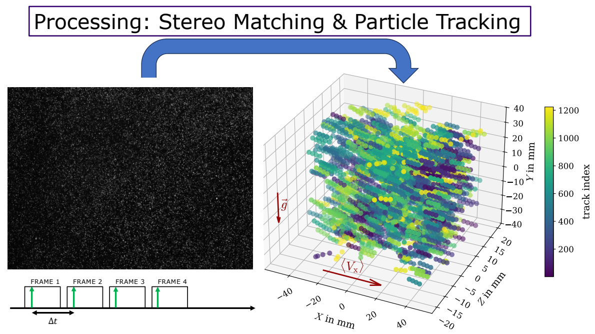

Figure 2. Processing pipeline from raw camera images that capture the scattered laser light from the particles to the 3D particle tracks. 1.) Detecting the particle positions in the camera frame. 2.) Stereo-matching of all camera views to retrieve 3D particle locations. 3.) Particle tracking over 4 consecutively captured frames.

Since simultaneous measurement of the turbulent flow field and particle dynamics is extremely difficult in this type of volume fractions, we conduct 1D-Pitot reference measurements of the carrier flow mean properties in the absence of particles. Since we take measurements under dilute conditions, the assumption that the turbulence statistics are not significantly altered by the presence of particles holds. We take measurements at different locations moving from the turbulent to the non-turbulent region, see figure 3. At the interface, we measure turbulent intensities greater than 10%. The Kolmogorov scale in the interface region for this wind tunnel in a similar grid configuration was measured by Ferran *et al.* (2024), yielding a Kolmogorov length scale of 250-300 µm and most particle Stokes numbers $St < 2$ in the interface region. In the non-turbulent region, we observe a bimodal distribution in the 1D mean streamwise velocity measurements. The lower velocity mode corresponds to the non-turbulent background flow by the fan system of the wind tunnel, while the high velocity mode corresponds to high turbulence entrainment events, transporting turbulent fluid into the non-turbulent region.

RESULTS

In the postprocessing of our data, we focus on particle statistics potentially influenced by gravitational acceleration, such as particle transport across the interface and settling behavior, as well as relative particle velocities, which are impor-

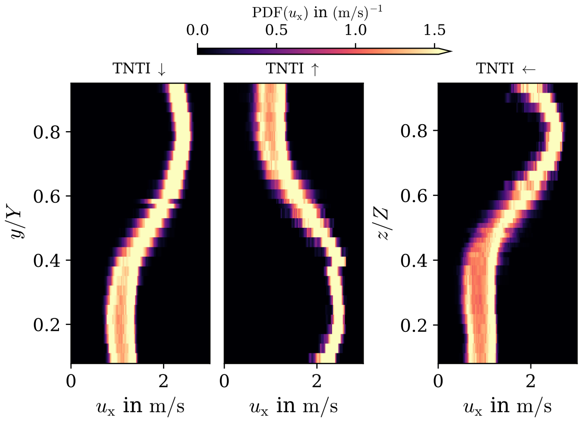

Figure 3. 1D flow speed measurements of the carrier flow turbulence from the turbulent to the non-turbulent side. At each location we plot the PDF of the mean stream velocity, revealing the bimodal distribution in the non-turbulent region caused by intermittent events.

tant for collision processes. Although the individual snapshots of the flow are independent of each other, the statistics of each snapshot can be influenced by entrainment events. Therefore, we condition each particle track on bursts following Blackwelder & Kaplan (1976), who set the burst threshold to a multiple of the local variance.

$$\frac{|\, v_x - \langle u_x \rangle \,|}{u'_{x,\mathrm{rms}}} = \begin{cases} \text{burst}, & \text{if } > C \\ \text{no burst}, & \text{if } \leq C \end{cases} \qquad (1)$$

Where $\langle u_x \rangle$ is the carrier flow mean fluid velocity, $u'_{x,\mathrm{rms}}$ is the standard deviation at the location of the measurement volume, and v_x is the particle velocity. The threshold C was set to 1.5 to balance the number of tracks belonging to bursts and no bursts, without only sampling extreme events. In the comparison of probability density functions (PDFs) between particle tracks and carrier phase mean stream velocities (Figure 4), we can see the tracks that belong to bursts. We can already see that in TNTI↓ and TNTI←, the particles show only a slightly higher mean stream velocity, and there is an even split between particles in bursts and those out of them. For TNTI↑, we can see that most tracks belong to burst events, showing a higher mean velocity, suggesting that they originate from deep in the turbulent region, being transported up by an entrainment event.

Particle Transport and Settling

By looking at the mean velocity of particles across the interface, we can estimate how the interface orientation influences particle transport from the turbulent to the non-turbulent region. Since we use the same operating conditions for all three cases, the total particle concentration in the wind tunnel is the same across them. Therefore, we can multiply the number of tracks by the mean velocity to get a property similar to a ”mass transport” across the interface (Figure 5). Across all cases, we can see that bursts cause the strongest transport to the non-turbulent region, with the strongest transport for TNTI↓. The transport for TNTI← is slightly higher compared to TNTI↑. This suggests that transport is affected by gravitational acceleration, even for high turbulence events. The influence of high turbulence events on particle transport agrees with

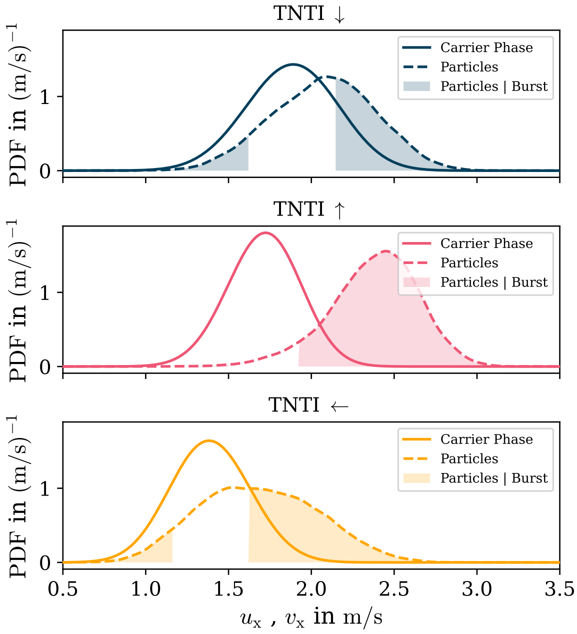

Figure 4. Comparison between mean streamwise velocities of particles and carrier flow at the location of the measurement volume to condition the particle data into burst events.

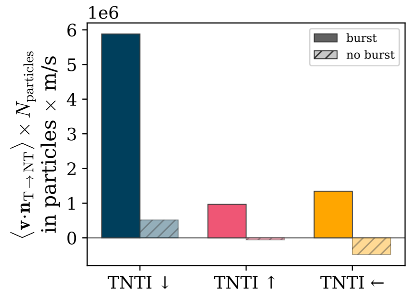

Figure 5. Comparison of particle transport from turbulent to non-turbulent region for the different cases, conditioned on bursts.

observations Good *et al.* (2012). It should be noted that particle diameters cannot be measured in particle tracking; therefore, we cannot conclude which particle sizes are being transported. This requires further investigation with PDPA measurements.

The conditioning can also be performed for the particles' settling velocity (Figure 6). We see that particles follow a similar distribution outside of bursts, with a mean settling velocity slightly lower than that of 20μm water droplets in air (-0.12 m/s). All distributions show wide tails reaching into regions of settling enhancement and hindrance. The presence of bursts significantly changes the settling velocity distribution for TNTI↓ and TNTI↑, while it only slightly shifts the distribution towards hindering for TNTI←. For TNTI↓, we observe a strong shift and slight skewness of the distribution towards enhancement, while we observe hindrance for TNTI↑. Additionally, we observe a narrowing of the distribution for TNTI↑ that isn't apparent in the other cases. The narrowing of the distribution could hint at the transport of a narrower droplet-size distribution by turbulent eddies, which filter out larger, heavier particles in the upward motion due to their mass.

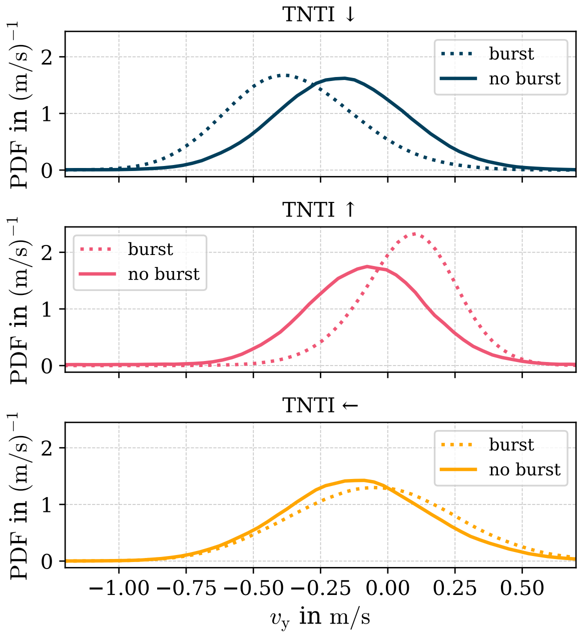

Figure 6. Comparison of particle settling velocities at the theoretical location of the interface conditioned on bursts.

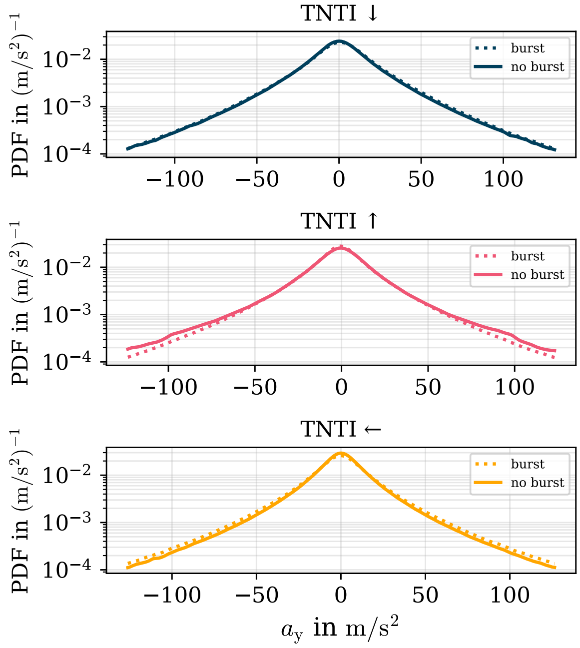

Figure 7. Comparison of vertical particle acceleration at the theoretical location of the interface conditioned on bursts.

Particle Acceleration

Looking at the acceleration statistics reveals insights on the effect of gravitational acceleration on droplet dynamics (Figure 7). The largest possible acceleration observed in particle tracking is limited by the search window size in the method. Therefore, our data is bound to accelerations of ± 100 m/s^2. We look at the vertical acceleration component of our data, since the gravitational acceleration acts on it. By looking only at the PDFs of the particles' acceleration components, the distributions appear to follow a similar pattern across all cases. We observe that bursts alter the probability of large accelerations for TNTI↑ and TNTI← only slightly. The probability for large accelerations decreases for TNTI↑, while it increases for TNTI← during bursts.

To understand the impact of the interface orientation on the acceleration statistics, we look at the moments of the distribution, for the unconditioned, as well as the burst-conditioned, data (Figure 8). We observe different mean accelerations across the three cases. The acceleration of TNTI← is close to zero, independent of conditioning. This could be explained by the fact that the large flow structures in this interface orientation have no preferential orientation in the z-direction, and the drag force on the particles is balanced by gravity. For TNTI↑, we can observe a negative mean acceleration that does not depend on the burst conditioning, while we observe a positive mean acceleration for TNTI↓, which gets closer to zero without the presence of bursts. These observations indicate that particles being flung upwards by the large eddies have, on average, experienced greater negative (downwards acceleration, since the vertical drag force that was acting on the particles as they moved up across the interface suddenly decreases once the particles are centrifuged out of the large eddy and enter the low turbulence side of the T-NT and gravitational acceleration is suddenly felt by the particles as they evolve into reaching their terminal (downwards) velocity. For TNTI↓, we observe the opposite mechanism at work, and the opposite result. During periods of bursts, the particles show a strong positive acceleration, which could hint at a stronger drag force acting on the particles when they interact with the non-turbulent fluid, since they far exceed their natural settling velocity. The fact that the positive acceleration is smaller during non-burst periods supports that theory, as the particles only have a slightly enhanced settling velocity then. The standard deviation of the acceleration is almost the same for all three cases, independent of the burst conditioning. Since the particle acceleration is directly related to the interaction with the turbulent flow structures, primarily through drag, we can then assume that the particles generally interact with the same range of flow structures. We can observe a slight increase in the standard deviation for TNTI↑ outside of bursts. Looking at the distribution's skewness, we observe that all cases have positive skewness, indicating that the distributions slightly lean towards negative accelerations. This indicates the general impact of gravitational acceleration on the particles. As with standard deviation, all distributions show similar kurtosis. We can see that all distributions exhibit higher kurtosis than a normal distribution ($\kappa = 3$), with slightly higher values for TNTI↑ and TNTI←.

Relative Particle Velocities

To analyze the impact of the interface orientation on potential particle collisions, we take a look at the relative velocity between particles in close proximity, as it is only meaningful to consider relative particle velocities in a small region around each particle. Therefore, we evaluate particle interactions within a radial distance of $\approx 10\ \eta$. This radius was chosen because we know that particles tend to form clusters of sizes of this size ($10\eta \approx 3$ mm for $\eta \approx 300\ \mu$m). We determine the closing speed and closing time of two particles by evaluating:

$$v_{\text{closing}} = \frac{\Delta\vec{v} \cdot \vec{r}_{\text{ij}}}{\|\vec{r}_{\text{ij}}\|} \qquad t_{\text{closing}} = \frac{\|\vec{r}_{\text{ij}}\|^2}{\Delta\vec{v} \cdot \vec{r}_{\text{ij}}} \tag{2}$$

for each particle interaction within the radius of influence. By analyzing the mean closing velocity of the particles around

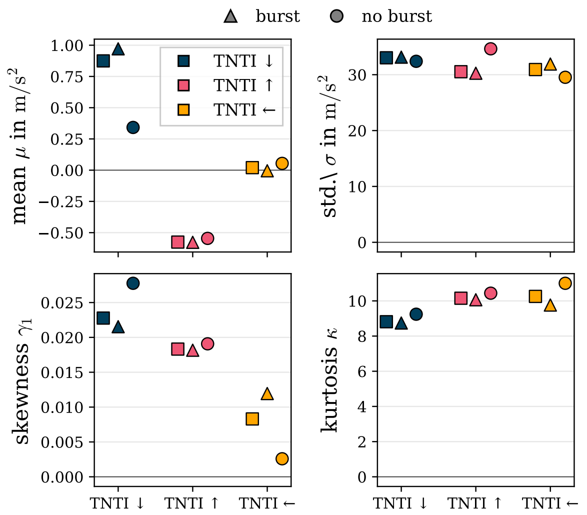

Figure 8. Comparison of statistical moments of the vertical particle acceleration (Fig. 7) at the theoretical location of the interface, comparing unconditioned and burst conditioned statistics.

each particle, we can determine if the particle-laden region around the particle (which could be a cluster) is contracting or expanding. This provides critical information about the clustering dynamics for different gravity orientations with respect to the T-NT interface. A mean negative closing velocity around the particle means that surrounding particles are moving towards the particle, decreasing the radial distance to the particle. A positive closing velocity, on the other hand, means that the particles around the reference particle are diverging, increasing their radial distance. We can observe the highest probability for large particle closing velocities for TNTI↑. For TNTI←, we observe a much higher probability for intermediate closing velocities, compared to the other gravity orientations. This could indicate that the dynamics of cluster formation and breakup depend strongly on gravity: Large positive relative velocities are more likely to bring particles together to form a cluster, while large negative relative velocities are more likely to lead to a cluster breakup. This suggests that the formation and breakup processes are more dynamic in the case of TNTI↑, while clusters are less likely to form and break up for TNTI↓. The mean relative distance between particles gives us additional information about the clustering of particles. From the PDF, we see that it's most likely to find particles at a radial distance of around 2.25 mm, which is the highest for TNTI↓. Additionally, we can observe that the probabilities for small radial distances are higher for TNTI↑ and TNTI← than for TNTI↓.

To analyze which particle pairs are most likely to collide with each other, we plot the distribution of closing times for particle pairs for which $\Delta v \cdot r < 0$ and pick the pair with the minimal time for each particle. Collisions for particles that contribute to the right side of the distribution with very large closing times are very unlikely, since there are much faster fluid timescales that will redistribute the particles. For very short closing times, particle collisions become more likely. We can see that we have a high likelihood for closing times around $4 \cdot 10^{-3}$ s, which is slightly smaller than the Kolmogorov timescale of $\tau_\eta \approx 6 \cdot 10^{-3}$ s. We can observe that the cases TNTI↓ and TNTI← have a higher likelihood for very small closing times, resulting in a higher probability of

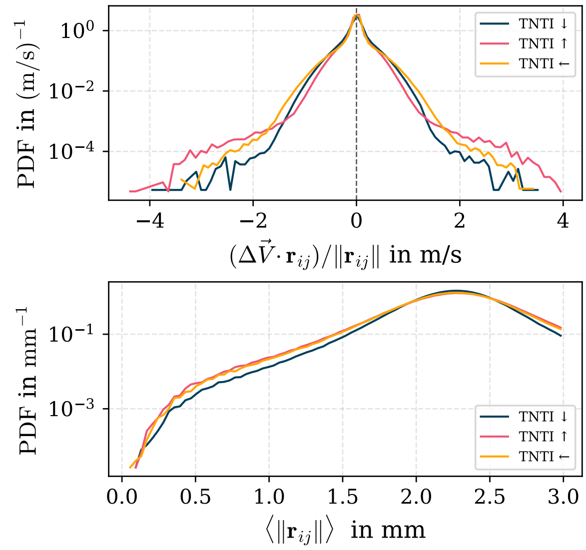

Figure 9. (1) Comparison of mean closing velocities in a small region around a particle (3 mm $\approx 10\eta$), revealing the distribution of contracting (positive closing velocities) vs. expanding particle (negative closing velocities) regions. (2) Comparison of the mean interparticle distance inside the region of influence for particles.

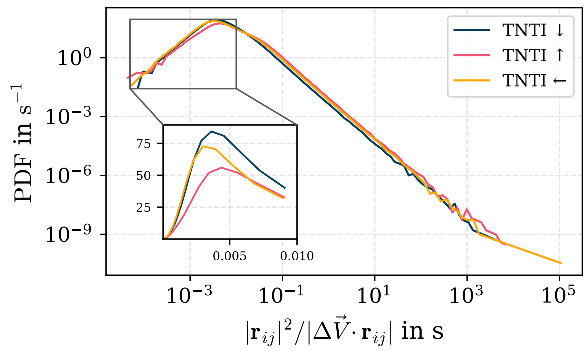

Figure 10. Comparison of the closing time of most probable colliding particle pairs in a 10 η neighborhood of particles.

particle-particle collisions.

It should be noted that these results show a general trend in particle closing times. Due to spatial resolution limits in the particle tracking, we have a minimal detectable particle distance in the particle tracking. This distance is limited by the cameras' ability to detect particles that are very close to each other as separate particles (in our case, around 100 μm), and still successfully stereo-match their 3D positions. We can expect that there are particles with even smaller interparticle distances, which might be much more likely to collide with each other.

Conclusion

These experimental results give us more detailed insights into the particle dynamics in TNTI and on the influence of gravitational acceleration on the particle dynamics. Through advanced particle tracking techniques, we measured accurate particle velocity and acceleration statistics over a large number of tracks collected over many large eddy turnover times. By conditioning our data on burst events, we investigate the influence of high turbulence, entrainment, and intermittent events on particle dynamics. In agreement with previous studies, we find that high turbulence events dominantly contribute to the transport of particles to the non-turbulent side. The effect of gravitational acceleration enhances or hinders this effect depending on the orientation to the interface. We additionally show that the orientation of gravity with respect to the interface impacts the settling behavior of particles, with the distribution shifted towards either hindering or enhancement of settling. However, gravitational acceleration can also have a filtering effect on the particles, as seen in TNTI↑. Most notably, we observe changes in the statistical moments of acceleration for the different orientations, a phenomenon that has not previously been reported by Good *et al.* (2012). Based on the relative particle velocities, we can make some estimates about the clustering dynamics in the presence of a T-NT interface, revealing a larger probability for high relative particle velocities in TNTI↑, which could hint at highly dynamic cluster formation and breakup. Lastly we looked at the most probable candidates for particle-particle collisions, and found that probabilities for short closing times are highest for TNTI↓.

REFERENCES

Aliseda, A., Cartellier, A, Hainaux, F. & Lasheras, J. C. 2002 Effect of preferential concentration on the settling velocity of heavy particles in homogeneous isotropic turbulence. *Journal of Fluid Mechanics* **468**, 77–105.

Bateson, C. P. & Aliseda, A. 2012 Wind tunnel measurements of the preferential concentration of inertial droplets in homogeneous isotropic turbulence. *Experiments in fluids* **52** (6), 1373–1387.

Blackwelder, RF & Kaplan, RE 1976 On the wall structure of the turbulent boundary layer. *Journal of Fluid Mechanics* **76** (1), 89–112.

Clark, A., Machicoane, N. & Aliseda, A. 2019 A quantitative study of track initialization of the four-frame best estimate algorithm for three-dimensional lagrangian particle tracking. *Measurement Science and Technology* **30** (4), 045302.

Ferran, A., Machicoane, N., Aliseda, A. & Obligado, M. 2023 An experimental study on the settling velocity of inertial particles in different homogeneous isotropic turbulent flows. *Journal of Fluid Mechanics* **970**, A23.

Ferran, A., Obligado, M. & Aliseda, A. 2024 Inertial particles in a turbulent/turbulent interface. *International Journal of Multiphase Flow* **179**, 104911.

Good, GH., Gerashchenko, S. & Warhaft, Z. 2012 Intermittency and inertial particle entrainment at a turbulent interface: the effect of the large-scale eddies. *Journal of fluid mechanics* **694**, 371–398.

Huck, P. D., Bateson, C., Volk, R., Cartellier, A., Bourgoin, M. & Aliseda, A. 2018 The role of collective effects on settling velocity enhancement for inertial particles in turbulence. *Journal of Fluid Mechanics* **846**, 1059–1075.